Civil Engineering Faculty Publications   Civil Engineering

5-2014

Nanoindentation Test Integrated with Numerical Simulation to Characterize Mechanical Properties of Rock Materials

Hoki Ban
Hanyang University, banhoki@hanyang.ac.kr

Pravat Karki
University of Nebraska - Lincoln, pravatko@utexas.edu

Yong-Rak Kim
University of Nebraska - Lincoln, yong-rak.kim@unl.edu

Hoki Ban,[1] Pravat Karki,[2] and Yong-Rak Kim[3]

Nanoindentation Test Integrated with Numerical Simulation to Characterize Mechanical Properties of Rock Materials

Hoki Ban,[1] Pravat Karki,[2] and Yong-Rak Kim[3]

Nanoindentation Test Integrated with Numerical Simulation to Characterize Mechanical Properties of Rock Materials

ABSTRACT

It is important to determine the mechanical properties of rock materials accurately from the viewpoint of the design, analysis, and modeling of various transportation infrastructure systems. Conventional methods have some drawbacks, including relatively inaccurate measurements, cumbersome testing-analysis processes, and high variability in measurements. A nanoindentation test integrated with a numerical modeling technique has been validated in other fields as an efficient and accurate tool for the characterization of the key mechanical properties of various irregularly shaped materials, such as the rock materials in this study. This paper presents an integrated experimental-numerical effort based on the nanoindentation measurement and finite-element modeling of a representative rock material, limestone. The experimental efforts, including specimen fabrication and laboratory tests, are presented, and the corresponding analyses of test results combined with the finite-element technique and linear interpolation to evaluate the property measurements are discussed. The elastic properties estimated from the nanoindentation test are similar to the simulation results, demonstrating the validity of the test method and modeling approach. The success of the proposed approach should facilitate the better design of mixtures and structures based on the more accurate characterization of the core material properties.

[1] Research Professor, Dept. of Civil and Environmental Engineering, Hanyang Univ., Seoul, 133-791, Republic of Korea, e-mail: banhoki@hanyang.ac.kr

[2] Ph.D. Student, Dept. of Civil Engineering, 362D Whittier Research Center, Univ. of Nebraska, Lincoln, NE 68588, United States of America, e-mail: pravatko@huskers.unl.edu

[3] Associate Professor, Dept. of Civil Engineering, 362N Whittier Research Center, Univ. of Nebraska, Lincoln, NE 68583, United States of America (Corresponding author), e-mail: ykim3@unl.edu

Introduction

Rock materials are widely used in civil engineering applications. Therefore, it is important to determine the mechanical properties of rock materials accurately from the viewpoint of design, analysis, and modeling. Mechanical properties including strength, stiffness, hardness, Poisson's ratio, and fracture toughness have been estimated by conventional test methods that mostly use bulk cores of rock samples. However, these conventional methods often yield somewhat inconsistent or inaccurate measurements that are frequently influenced by the testing personnel, sample preparation process, and/or specimen quality. This subsequently results in high variability in the measurements and increased costs because multiple bulk core replicates are required to obtain statistically acceptable results. As such, there is a strong need for an alternative method that can overcome, at least partially, the drawbacks of conventional methods. Such a method should be scientific, consistent, accurate, reliable, and practically efficient.

Any combination of sand, gravel, and crushed stone in its natural or processed state is typically referred to as an aggregate. Aggregates are used in the field of transportation infrastructure for the construction of highways, airfields, parking lots, storage areas, and ballast or subballast layers in railroad track structures. Aggregates are the main phases in such transportation infrastructure, and, therefore, it is significant to accurately estimate their mechanical properties to reach better design and performance analysis of the various transportation infrastructure systems. In particular, in recent times, micromechanical approaches have been actively studied [1–5] because they offer various advancements over conventional phenomenological approaches. Micromechanical approaches have demonstrated that mixture properties are directly affected by accuracy of component properties. For example, asphalt mixtures in pavements are usually modeled as heterogeneous composites of two distinct phases—elastic aggregates and viscoelastic matrix—to predict their overall stiffness and fracture characteristics. Zhou et al. [6] and Aragão et al. [5] have shown that the elastic modulus of aggregates significantly influences the overall stiffness and strength of mixtures. However, despite the importance of the accurate measurement of the aggregate mechanical properties, suitable test methods for this purpose have not yet been actively explored.

Nanoindentation is a simple technique for characterizing a material in which a material of unknown properties is subjected to force- or displacement-controlled penetration using a comparatively harder indenter of known geometry and mechanical properties. The instantaneous load and displacement results from the specimen can be interpreted to determine some important mechanical properties such as the Young's modulus [7,8], hardness [7,8], inelastic properties [9], and fracture properties [10,11]. Recently, nanoindentation techniques have been widely used to characterize diverse materials such as steel, aluminum, human tissue, and bone [12–14] as well as various civil engineering materials [15–18].

Experimental nanoindentation techniques have often been integrated with some numerical techniques—finite element modeling is used most often. This is because finite element modeling can provide an efficient tool to help understand the indentation process itself or to characterize unknown mechanical properties from the nanoindentation test data. Occasionally, it is not feasible to simply extract material properties from the experimentally obtained load-displacement curve. Therefore, many studies [19–24] have used the finite element method to determine various mechanical properties of materials by fitting the simulated loading–unloading curves to the experimentally obtained ones.
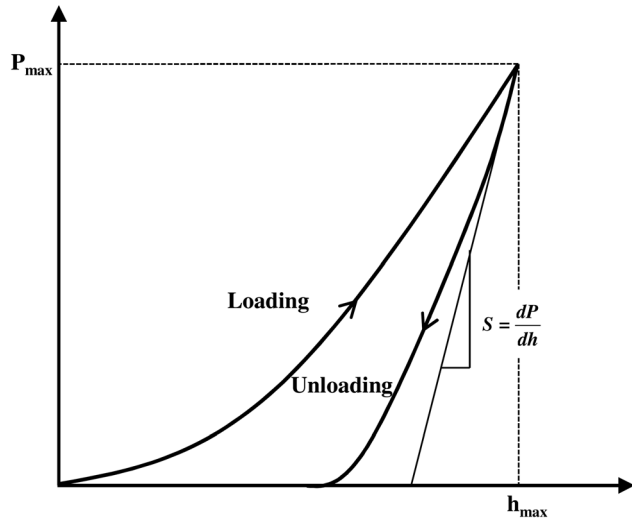
Study Objectives and Scope

The primary objective of this study is to explore an innovative and advanced technique, compared with conventional methods, for the measurement of the mechanical properties of rock materials, including aggregates. Doing so may facilitate the better design of mixtures and structures based on a more accurate characterization of material properties. Toward this end, this study integrates the laboratory nanoindentation test with numerical modeling based on the aforementioned seminal studies in this field. As a part of this particular effort, instead of expanding the scope, only one type of rock material, limestone, was selected to investigate the consistency of nanoindentation tests and the validity of numerical modeling. It is important to ultimately seek a statistically satisfactory estimation of the mechanical properties of a material.

Nanoindentation Method

A nanoindentation measurement is performed by pushing an indenter into a specimen and then withdrawing it; when doing so, the force and corresponding displacement are continuously recorded. **Figure 1** shows a typical load-displacement curve obtained from nanoindentation testing. It shows the peak load P_{max}, maximum displacement depth h_{max}, and contact stiffness S which is an initial slope of the unloading curve. The measured force as a function of the indented depth during loading is characteristic of the resistance of the sample to deformation, including both elastic and plastic deformations. During unloading, the decrease in force with depth is governed by the elastic response of the sample. The initial derivative of the force with respect to depth during initial unloading is defined as the contact stiffness S at that depth.

Over the last few decades, several approaches have been developed to analyze nanoindentation data [8,13,25,26]. Among

FIG. 1   Typical load versus indenter displacement showing parameters required to determine the hardness and elastic modulus.

FIG. 2   Schematic diagram of indentation (h, indenter displacement; h_c, contact depth; h_{max}, max displacement; P, force applied to indenter).

these, the Oliver-Pharr method [8], which is based on the studies by Doerner and Nix [7] and Sneddon [27], is most commonly used because it is well established to determine the elastic modulus and hardness of materials. Therefore, the Oliver-Pharr method was adopted to analyze the nanoindentation test results in this study.

The mechanical properties, i.e., hardness and Young's modulus, are computed from three measured parameters: peak load P_{max}, maximum displacement h_{max}, and contact stiffness $S = dP/dh$. The first two values can be obtained directly from the load-displacement data, and the third is determined by curve fitting the upper portion of the unloading curve and measuring its slope at peak load. With these parameters, the first step in the computing process is to determine the contact depth h_c, as schematically illustrated in **Fig. 2**. The contact depth is determined from the following relation:

(1)
$$h_c = h_{max} - \varepsilon \frac{P_{max}}{S}$$

where:

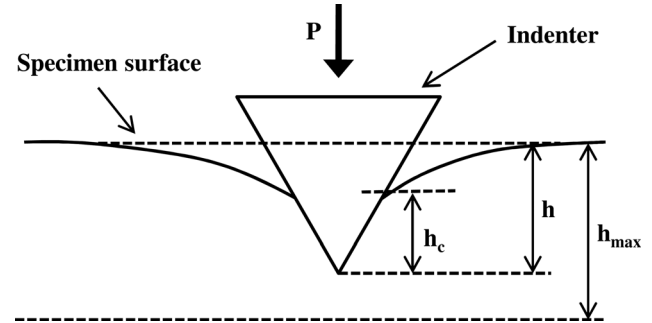$\varepsilon =$ a geometrical constant associated with the shape of the indenter.

Among several different types of indenters, a three-sided pyramidal Berkovich indenter made of diamond was used for the nanoindentation tests in this study. The geometrical constant ε of this indenter is 0.75 [8].

Once h_c is determined, the projected area A_c of actual contact can then be calculated using the cross-sectional shape of the indenter along its length. This area function could be determined by the direct measurement of the indenter using a scanning microscope; however, in practice, it is normally determined by indenting a known sample and iteratively fitting the

results. For example, the projected area A_c for a Berkovich indenter can be expressed as a function of h_c as follows [28]:

(2)
$$A_c = 24.5h_c^2 + C_1h_c + C_2h_c^{0.5} + C_3h_c^{0.25} + ...$$

where:

the coefficients $C_i =$ adjustable coefficients determined through best fitting to the experimental data during the calibration process,

the first term = the area versus depth for a perfectly sharp Berkovich indenter, whereas

the second term accounts for tip blunting.

After the area is computed, the hardness is then simply computed as follows:

(3)
$$H = \frac{P_{max}}{A_c}$$

The final step in the computing process is to determine the elastic modulus. Pharr et al. [29] have shown that Sneddon's solution [27] can be adopted independently of the geometry of the indenter, leading to the following equation for an elastic modulus:

(4)
$$E_r = \frac{1}{\beta} \frac{\sqrt{\pi}}{2} \frac{S}{\sqrt{A_c}}$$

where β is a small correction factor for the non-axisymmetric indenter shape ($\beta = 1.034$ [8] for a Berkovich tip).

To account for the elastic response of the indenter, the elastic modulus in Eq. (4) is assumed to be a reduced modulus defined as follows:

(5)
$$\frac{1}{E_r} = \frac{1 - \nu_s^2}{E_s} + \frac{1 - \nu_i^2}{E_i}$$

where E_s and ν_s are the Young's modulus and Poisson's ratio of the specimen and E_i and ν_i are the Young's modulus and Poisson's ratio of the indenter. The Young's modulus and Poisson's ratio of the diamond used in the Berkovich indenter is 1141 GPa and 0.07, respectively.

Specimen Preparation and Test

In this study, limestone was selected for nanoindentation tests as a representative rock material used in civil engineering. Limestone used in this study was obtained from a local quarry in Nebraska, United States. The bulk specific gravity and absorption capacity were measured as 2.624 and 1.25 %, respectively. Limestone specimens were prepared by cutting a large limestone rock into thin slices with approximate dimensions of 10 mm × 10 mm × 5 mm. Because the accuracy of the elastic modulus and hardness values determined from the nanoindentation tests is directly dependent on the accuracy of the contact area, it is imperative to avoid any errors because of uneven specimen surfaces [30,31]. Therefore, these small limestone specimens were subjected to several grades of abrasive grinding and polishing sandpapers to smoothen the rough surfaces. The specimens were then polished with sub-micron colloidal alumina suspensions (1.0, 0.3, and 0.05 μm in sequence) on specially fabricated polishing cloths. During the entire grinding and polishing process, pure water was continuously fed to the specimens and substratum to wash away the particles polished off during grinding. The specimens were washed again with water before keeping them in the test chamber of the indentation equipment for better resolution during the tests.

In this study, the nanoindentation experiments provide in situ image and quantitative material characterization of the specimen's nanomechanical properties. Force is applied using electrostatic actuation, and a capacitive sensor is used to measure the displacement. The axis of the indenter is vertical, and the same transducer is used for both force application and displacement measurements. As mentioned previously, a Berkovich indenter made of diamond was used in this study. A typical Berkovich indenter has an aspect ratio of 1:8 and an average radius of curvature of 150 nm [32].

As is the case with most experimental systems, calibration is of importance because it limits uncertainties and results in a repeatable and reproducible experiment. Tip-shape calibration is based on the determination of an area function, as mentioned earlier. This method assumes that the specimen modulus is independent of the indentation depth. Fused silica with a Young's modulus of 72 GPa was used as a standard material for calibration. An area function relating the projected contact area (A_c) to the contact depth (h_c) was obtained by a series of indents at various contact depths. Test data were then used for a polynomial fitting as given by Eq 2, which resulted in the constants, C_i.

After the calibration process was completed, the prepared limestone specimens were securely placed at the central region of the stage inside the environmental chamber, with the target testing temperature of 21°C. The specimens in the environmental chamber were then viewed through an optical microscope to identify the different regions and the points of interest. A total of 40 indentation points, which is considered a sufficient number of data points for statistical analyses, were made in the specimens. In addition, sufficient distance was maintained between each indentation to avoid the unduly influences, if any, of neighboring indentations on the stiffness and hardness values.

In this study, two different indentation schemes were employed. First, nine indentations were made in the specimen using a force-controlled trapezoidal function, with 10 s of loading and 10 s of unloading each at 200 μN/s including an intermediate holding step of 10 s at a peak load of 2000 μN, as shown in **Fig. 3(a)**. The holding period was applied to allow creep, if any [33], so that the unloading data would have any effects of the viscoelastic behavior of limestone. The results did not show any creep at constant load, indicating that the limestone is fairly elastic. Based on this finding, the next 31 indentations were attempted using a displacement-controlled bilinear function without a holding period as illustrated in **Fig. 3(b)**.
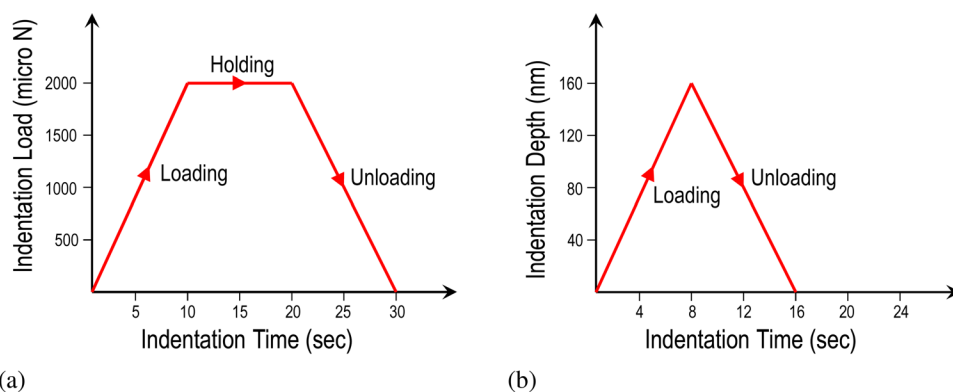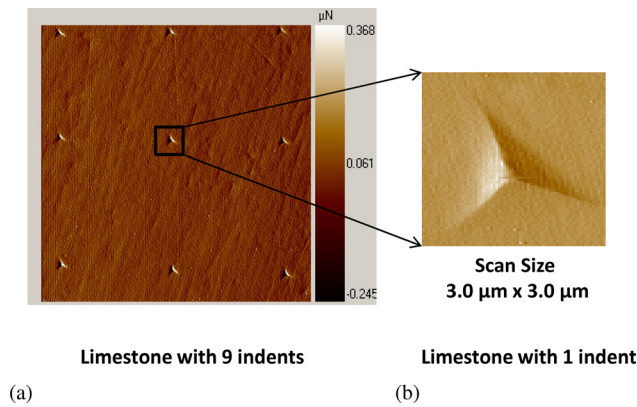
FIG. 3

Two loading schemes employed in this study.

FIG. 4   Images of residual depths in limestone.

Scan Size
3.0 µm x 3.0 µm

Limestone with 9 indents   **Limestone with 1 indent**

(a)   (b)

Test Results and Discussion

The residual impressions from the indentation performed using the three-sided Berkovich tip are shown in **Fig. 4(a)** at nine different indentation points. Similarly, a magnified view of one of the residual indentations is shown in **Fig. 4(b)**, which illustrates the partial recovery of indentation in two-dimensional (2D) configuration, when the indenter is taken away from the limestone specimen. As mentioned earlier, the elastic property of the specimen is related to the recovery portion.

Figure 5 shows a representative load-displacement curve resulting from the bilinear loading scheme. It is seen that the test result herein is very similar to the typical load-displacement curve of nanoindentation testing shown in **Fig. 1**. Three primary measurements: peak load, maximum penetration depth, and contact stiffness, could be readily identified from the curve. Then, as illustrated earlier, the hardness and reduced elastic modulus of each indentation were calculated by Eqs 3 and 4. After removing four outliers from the total 40 measurements,

FIG. 5   A representative nanoindentation test result: load versus displacement curve.
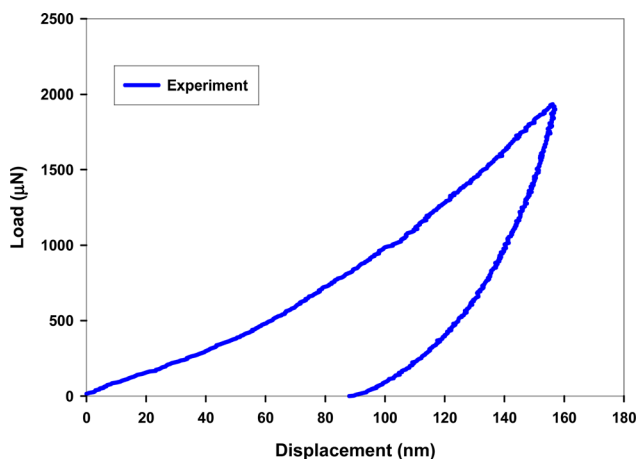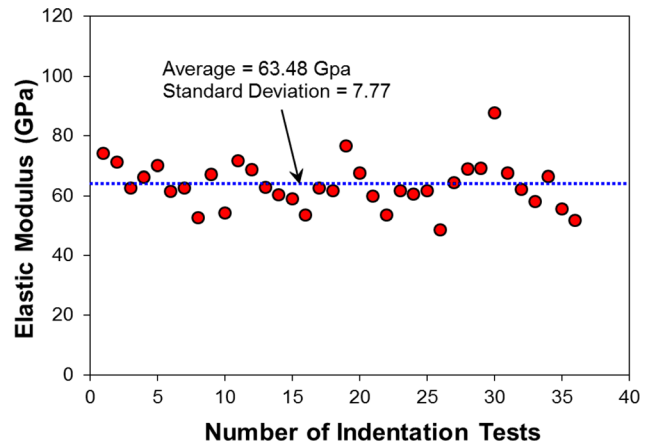

FIG. 6   Young's moduli obtained from the nanoindentation test.

the average values and standard deviations of the reduced elastic modulus and hardness were obtained as 66.12 ± 8.10 GPa and 2.30 ± 0.34 GPa, respectively. Finally, using Eq 5, the Young's moduli (E_s) was obtained as 63.48 ± 7.77 GPa, as shown in **Fig. 6**. A Poisson's ratio of 0.2 was reasonably assumed based on a previous study [6]. The Young's modulus found from the nanoindentation test appears that it is slightly larger than the upper bound value of conventional elastic modulus range of limestone, 30–60 GPa [34], with much smaller variability. The discrepancy might be because of a huge scale effect between the nanoscale test in this study and the conventional test using bulk cores of rock samples, although it needs further verification to be confirmed.
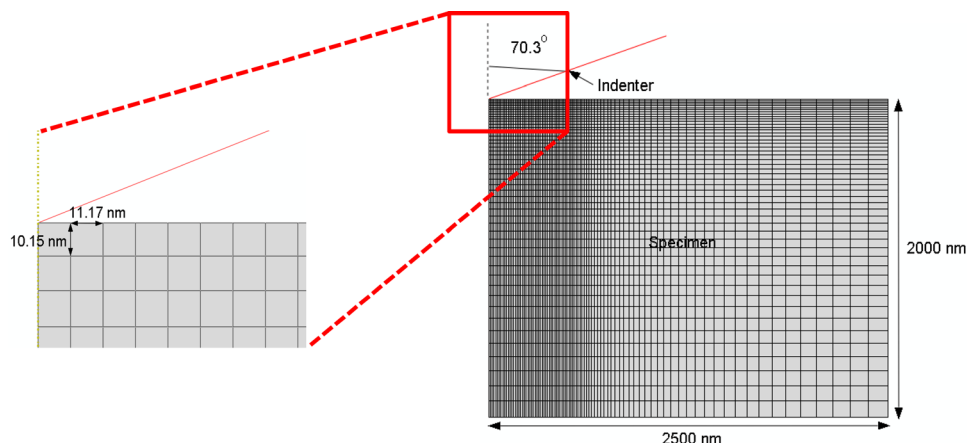
Finite Element Modeling

To evaluate the mechanical properties obtained from the laboratory nanoindentation tests, numerical modeling was also carried out by integrating the model simulation with tests. This process can successfully identify unknown material properties of the limestone by targeting good agreements between the laboratory test results and the numerical simulations. This integrated experimental-numerical approach was adopted by employing a finite element technique.

Toward this end, 2D axisymmetric modeling was conducted using a commercial finite element software, ABAQUS [35]. In the finite element modeling, the triangular Berkovich indenter was geometrically represented by a movable rigid cone whose half-included tip angle is 70.3°. This provides the same depth-to-area ratio as the Berkovich pyramid used in the actual tests. It should be noted that the 2D axisymmetric modeling with a rigid cone indenter is limited to truly simulate indentation process of the Berkovich tip; however, the 2D approximation was adopted at this stage to reduce computational complexities induced by 3D contact. The limestone was

modeled by 4-node axisymmetric elements (CAX4 in ABA-QUS) because of its symmetry condition. **Figure 7** illustrates the finite element mesh in the region near the indenter tip. Because most of the deformation occurs immediately under the indented region, the highest mesh density was employed around the indenter tip, with each element having a size of 10.15 nm × 11.17 nm. Farther away from the contact area, a progressively coarser mesh was used to reduce the computational time. A total mesh extent of 2000 nm depth and 2500 nm radius was found to be sufficiently large to eliminate the edge (boundary) effect. Horizontal displacements along the axis of symmetry and vertical displacements at the bottom of the specimen were constrained.

The limestone was modeled as an isotropic, elastic-plastic solid. Among various plasticity models, this study employed the Drucker-Prager model, because it is often used for modeling rocks and soils. The Drucker-Prager yield criterion is a simple modification of von Mises yield criterion. The influence of a hydrostatic stress component on failure is introduced by inclusion of an additional term in the von Mises expression as follows:

$$f(I_1, J_2) = \sqrt{J_2} - \alpha I_1 - K = 0 \tag{6}$$

where I_1 and J_2 are the first and second invariant of stress tensor, respectively, and α and K are material constants that are represented as follows:

$$\alpha = \frac{2 \sin \phi}{\sqrt{3}(3 - \sin \phi)} \tag{7}$$

$$K = \frac{6C \cdot \cos \phi}{\sqrt{3}(3 - \sin \phi)} \tag{8}$$

where ϕ is the angle of internal friction and C is the cohesion of material.

Model Simulation Results

Two subsequent steps, loading and unloading, were simulated. During loading, the rigid cone indenter moves downward along the axis of symmetry to penetrate the specimen at an indentation rate of 20 nm/s. During unloading, the indenter returns to its original position at the same rate. It should also be noted that the indenter's maximum displacement is set to be 160 nm, which is the same limit as that applied to the actual measurements. **Figure 8** shows the maximum principal stress contours at three different loading stages (A: stage at 90 nm indentation, B: stage at the peak load, and C: stage at the end of unloading). The figure clearly shows that the deformation is concentrated at the area near the indenter tip, and the specimen is subjected to both elastic recovery and plastic deformation at the end of simulation, which can be observed from the actual test as shown in **Fig. 4**.

For the experimental-numerical integration, this study employed the approach by Knapp et al. [23], because it is practically efficient and is based on statistical concepts to obtain a good fit between experiments and simulations. First, several arbitrary simulations (typically, a set of three or more) were conducted with different sets of the material properties (i.e., Young's modulus (E) and material cohesion (C) for the Drucker-Prager model). The two material properties were selected as unknown (calibrated) properties because the indentation test is quite sensitive to changes in either E or C with the loading portion sensitive to both and the unloading primarily sensitive to E. Therefore, the internal friction angle of limestone (ϕ) was assumed with a representative value of 35° based on the literature [36]. A total of four arbitrary simulations were conducted. **Figure 9** shows the simulation results of the load-displacement curves. It also shows a load-displacement curve from the nanoindentation test for comparison. As seen in the figure, the four arbitrary simulations were intentionally

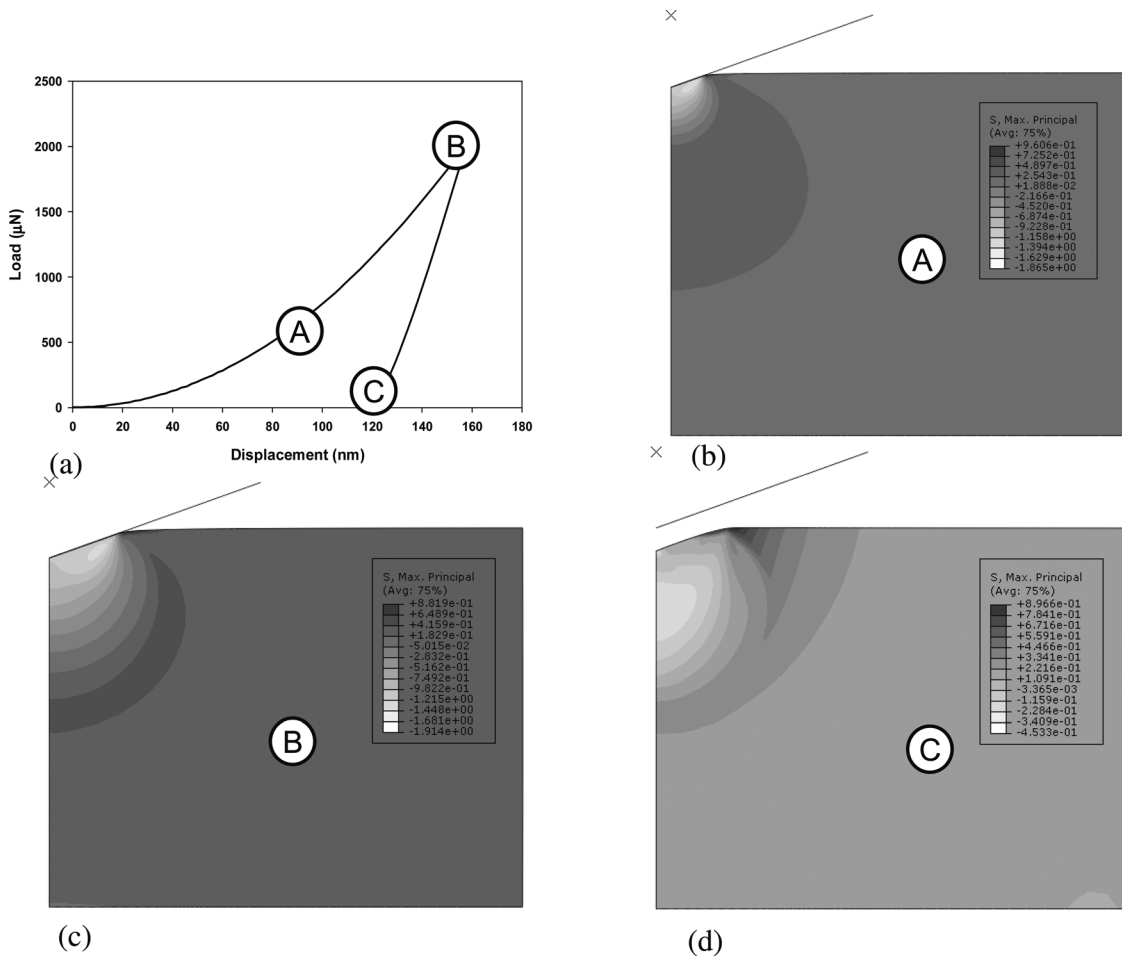**FIG. 8**   Maximum principal stress contour plots and deformations at three different loading stages.
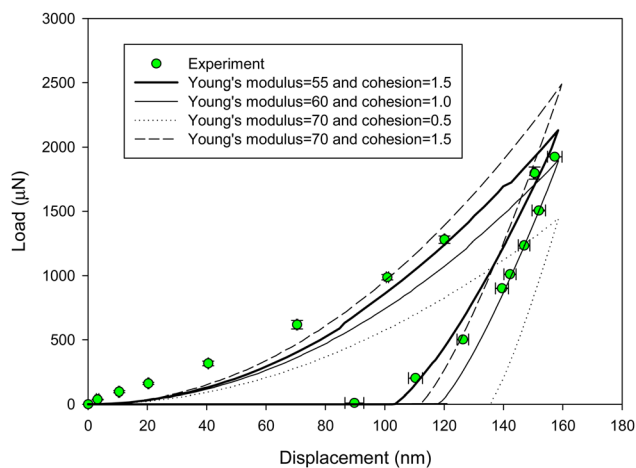

(a)

(b)

(c)

(d)

FIG. 9   Load-displacement curves from trial simulations and nanoindentation tests.

designed to bracket the expected material properties because the calibrated properties are found by an interpolation of the arbitrary cases that should be with the smallest number of trials. The properties found through this process are those that would be expected to enable a simulation to give a good (although not necessarily the best) fit to the experiment.

After the trial simulations were completed, the corresponding values of P_{max} and S that are obtained by curve-fitting short sections of the simulated data are compared to an averaged P_{max} versus S pair obtained from the experimental load-displacement curves. **Figure 10(a)** shows a hollow point representing the experimental force and stiffness and four filled points resulting from the four arbitrary simulations. The plot illustrates that the simulated P_{max} versus S pairs have bracketed the experimental value.

The next step is to use the P_{max} versus S pairs and each corresponding E and C to interpolate to new trial values for E and C. Each set of E and C is parameterized as a function of P_{max} and S. This is because the two mechanical properties (E and C)

FIG. 10 Results of the three-parameter linear interpolation analysis.

(a) P_{max} vs. S pairs

(b) E vs. C pairs
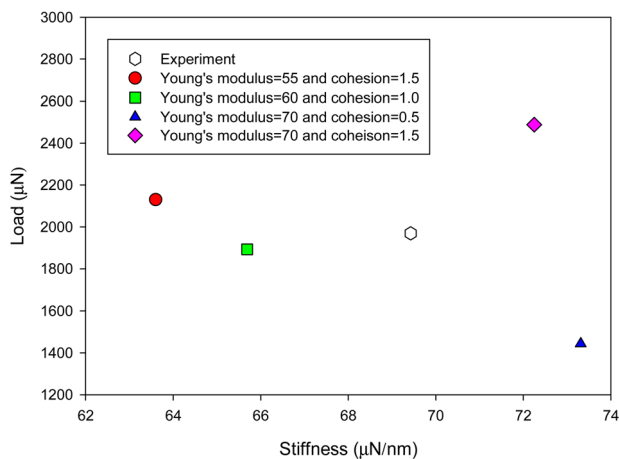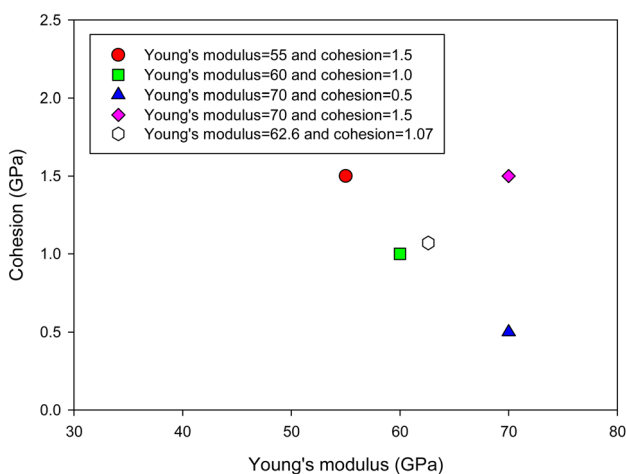
FIG. 11 Comparison between the best-fit simulation and experiments.

are strongly related to the peak load and contact stiffness by definition and physical observations. The following three-parameter linear interpolations are used in this study [23].

$$E = a_1 S + b_1 P_{max} + c_1 \qquad (9)$$

$$C = a_2 S + b_2 P_{max} + c_2 \qquad (10)$$

where a_1, a_2, b_1, b_2, c_1, and c_2 are model parameters.

The three-parameter linear interpolation is performed to find the best combination of E and C values. This procedure gives the predicted material properties that should result in a good match of the load-displacement between the simulated curve and the experimental curve. Applying this procedure resulted in a cohesion of 1.07 ± 0.51 GPa and a Young's modulus of 62.6 ± 5.84 GPa. The final E and C pair is plotted in
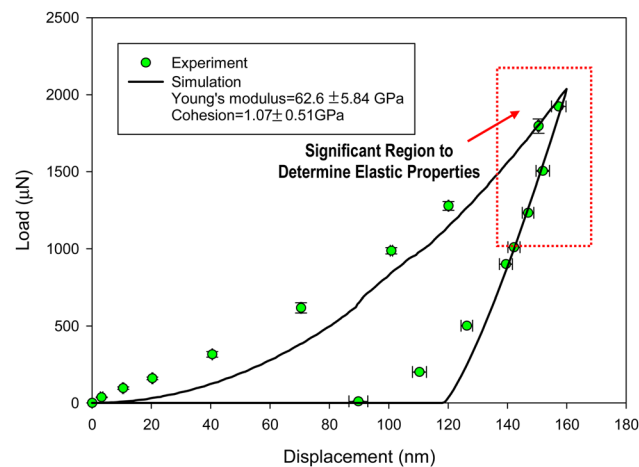
Fig. 10(*b*) with a hollow point that is surrounded by four filled points that indicate the *E-C* properties used for the simulations.

The final best-fit simulation is shown by a solid line in Fig. 11. Although it is the best fit, the loading part and the final stage of the unloading part of the simulation do not exactly follow the experiments, which implies that some other features may be necessary in the model for better agreement. However, the elastic behavior of limestone represented by the peak load and the initial unloading slope in the simulation agrees well with those from the experiments. This is confirmed when one compares the experimental E value (i.e., 63.48 ± 7.77 GPa) with the simulated E value (i.e., 62.6 ± 5.84 GPa) optimized from the interpolation process. Both values are very close within the limit of variation. The close agreement between the two integrated efforts—experimental and numerical—demonstrates the validity of the test method and numerical model.

Regarding another material parameter C, model simulation results were only compared to typical values found in literature [36], because nanoindentation tests did not produce the material cohesion. As presented in **Table 1**, the cohesion obtained from the model simulation appears that it is much larger (by approximately 50–150 times) than the typical cohesion value of limestone. The large discrepancy might be because of combined effects of model limitations and assumptions such as the 2D approximation in the finite element simulation and the use of the Drucker-Prager yield criterion that could not be completely compatible with the small scale nanoindentation process. Similar to the aforementioned discrepancy of the elastic modulus between test results and conventional values, the huge scale effect (nanometer scale indentation versus centimeter-meter scale test of bulk rock samples) needs to be further investigated, because there might be significant length- and time-related scale factors involved between the two.

TABLE 1   Physical and mechanical properties of limestone (conventional values, test results, and model simulation results).

Properties	Conventional Value [34,36]	Test Result	Model Simulation Result
Specific gravity	1.88–2.81	2.624	NA
Water absorption (%)	0.50–24.0	1.25	NA
Elastic modulus (GPa)	30–60	63.48 ± 7.77	62.6 ± 5.84
Poisson's ratio	0.18–0.33	0.20[a]	0.20[a]
Compressive strength (MPa)	18–193	NA	NA
Tensile strength (MPa)	2.90–5.88	NA	NA
Shear strength (kPa)	5.5–24.8	NA	NA
Cohesion (MPa)	6.72–23.6	NA	1070 ± 510
Friction angle (degree)	34.8–42	NA	35[a]

[a]Assumed based on literature.

Concluding Remarks

As an alternative to conventional test methods that present relatively inaccurate, inconsistent results and are cumbersome to perform for the characterization of the mechanical properties of rock materials, this study attempted an innovative approach in which a nanoindentation test was integrated with finite element modeling. Based on the test-model results, the following conclusions can be drawn.

- The presented nanoindentation approach provides an efficient and reliable tool for the characterization of the key mechanical properties of rock materials. The test results were generally consistent with a small standard deviation.
- A total of 40 indentations of limestone yielded an elastic modulus value of 63.48 ± 7.77 GPa. This experimental estimation was very close to the numerical simulation result: 62.6 ± 5.84 GPa. The close agreement between the two parallel efforts demonstrates the validity of the test method and modeling approach.
- Model simulation results of the strength- or failure-related material characteristics appeared a large discrepancy comparing to the conventional values. It clearly remains improvements of the model and further investigation of scale effects. Follow-up studies are recommended.
- Although additional tests, data analyses, and model features with an extended scope would be necessary to confirm the approach presented in this study, it is implied that the integrated experimental-numerical effort could overcome, at least partially, some of the drawbacks of conventional testing-analysis approaches.
- The success of the proposed approach should facilitate the better design of mixtures and transportation infrastructures based on more accurately characterized material properties.

References

[1] Dai, Q., Sadd, M. H., Parameswaran, V., and Shukla, A., "Prediction of Damage Behaviors in Asphalt Materials Using a Micromechanical Finite-Element Model and Image Analysis," *J. Eng. Mech.*, Vol. 131, No. 7, 2005, pp. 668–677.

[2] Guddati, M. N., Feng, Z., and Kim, Y. R., "Towards a Micromechanics-Based Procedure to Characterize Fatigue Performance of Asphalt Concrete," *Transport. Res. Rec.*, Vol. 1789, 2002, pp. 121–128.

[3] Souza, F. V., Soares, J. B., Allen, D. H., and, Evangelista, F., "A Model for Predicting Damage Evolution in Heterogeneous Viscoelastic Asphaltic Mixtures," *Transport. Res. Rec.*, Vol. 1891, 2004, pp. 131–139.

[4] Kim, H., Wagoner, M. P., and Buttlar, W. G., "Micromechanical Fracture Modeling of Asphalt Concrete Using a Single-Edge Notched Beam Test," *Mater. Struct.*, Vol. 42, No. 5, 2009, pp. 677–689.

[5] Aragão, F. T. S., Kim, Y., Lee, J., and Allen, D. H., "Micromechanical Model for Heterogeneous Asphalt Concrete Mixtures Subjected to Fracture Failure," *J. Mater. Civil Eng.*, Vol. 23, No. 1, 2011, pp. 30–38.

[6] Zhou, F. P., Lydon, F. D., and Barr, B. I. G., "Effect of Coarse Aggregate on Elastic Modulus and Compressive Strength of High Performance Concrete," *Cement Concrete Res.*, Vol. 20, 1995, pp. 177–186.

[7] Doerner, M. F. and Nix, W. D., "A Method for Interpreting Data from Depth-Sensing Indentation Instruments," *J. Mater. Res.*, Vol. 1, 1986, pp. 601–609.

[8] Oliver, W. C. and Pharr, G. M., "An Improved Technique for Determining Hardness and Elastic Modulus Using Load and Displacement Sensing Indentation Experiments," *J. Mater. Res.*, Vol. 7, 1992, pp. 1564–1583.

[9] Mayo, M. J. and Nix, W. D., "A Micro-Indentation Study of Superplasticity in Pb, Sn, and Sn-38 wt. % Pb," *Acta Metall.*, Vol. 36, 1988, pp. 2183–2192.

[10] Lawn, B. R., Evans, A. G., and Marshall, D. B., "Elastic/Plastic Indentation Damage in Ceramics: The Median/Radial Crack System," *J. Am. Ceram. Soc.*, Vol. 63, 1980, pp. 574–581.

[11] Harding, D., Oliver, W., and Pharr, G., "Cracking During Nanoindentation and Its Use in the Measurement of Fracture Toughness," *Mater. Res. Soc. Symp. Proc.*, Vol. 356, 1995, pp. 663–668.

[12] Tsui, T. Y., Oliver, W. C., and Pharr, G. M., "Influence of Stress on the Measurement of Mechanical Properties Using Nanoindentation. Part I: Experimental Studies in an Aluminum Alloy," *J. Mater. Res.*, Vol. 11, 1996, pp. 752–759.

[13] Hainsworth, S. V., Chandler, H. W., and Page, T. F., "Analysis of Nanoindentation Load-Displacement Loading Curves," *J. Mater. Res.*, Vol. 11, 1996, pp. 1987–1995.

[14] Gupta, S., Carrillo, F., Balooch, M., Pruitt, L., and Puttlitz, C., "Simulated Soft Tissue Nanoindentation: A Finite Element Study," *J. Mater. Res.*, Vol. 20, 2005, pp. 1979–1994.

[15] Constantinides, G., Ulm, F. J., and van Vliet, K., "On the Use of Nanoindentation for Cementitious Materials," *Mater. Struct.*, Vol. 36, 2003, pp. 191–196.

[16] Mondal, P., Shah, S., and Marks, L., "A Reliable Technique to Determine the Local Mechanical Properties at the Nanoscale for Cementitious Materials," *Cement Concrete Res.*, Vol. 37, No. 10, 2007, pp. 1440–1444.

[17] Ossa, E. A. and Collop, A. C., "Spherical Indentation Behavior of Asphalt Mixtures," *J. Mater. Civil Eng.*, Vol. 19, No. 9, 2007, pp. 753–761.

[18] Tarefder, R. A., Zaman, A. M., and Uddin, W., "Determining Hardness and Elastic Modulus of Asphalt by Nanoindentation," *Int. J. Geomech.*, Vol. 10(3), 2010, pp. 106–116.

[19] Poon, B., Rittel, D., and Ravichandran, G., "An Analysis of Nanoindentation in Elasto-Plastic Solids," *Int. J. Solids Struct.*, Vol. 45, 2008, pp. 6399–6415.

[20] Woodcock, C. L., Bahr, D. F., and Moody, N. R., "Plastic Zone Development Around Nanoindentations," *Mater. Res. Soc. Symp. Proc.*, Vol. 649, 2000, pp. 14–19.

[21] Xu, Z. and Li, X., "Sample Size Effect on Nanoindentation of Micro-/Nanostructures," *Acta Mater.*, Vol. 54, 2006, pp. 1699–1703.

[22] Bolshakov, A., Oliver, W. C., and Pharr, G. M., "Influence of Stress on the Measurement of Mechanical Properties Using Nanoindentation. Part II: Finite Element Simulation," *J. Mater. Res.*, Vol. 11, 1996, pp. 760–768.

[23] Knapp, J. A., Follstaedt, D. M., Myers, S. M., Barbour, J. C., and Friedmann, T. A., "Finite Element Modeling of Nanoindentation," *J. Appl. Phys.*, Vol. 85, 1999, pp. 1460–1474.

[24] Huang, X. and Pelegri, A. A., "Finite Element Analysis on Nanoindentation With Friction Contact at the Film/Substrate Interface," *Comp. Sci. Technol.*, Vol. 67, 2007, pp. 1311–1319.

[25] Cheng, Y. T. and Cheng, C. M., "Scaling Approach to Conical Indentation in Elastic-Plastic Solids With Work Hardening," *J. Appl. Phys.*, Vol. 84, 1998, pp. 1284–1291.

[26] Cheng, Y. T. and Cheng, C. M., "Scaling Relationships in Conical Indentation of Elastic-Perfectly Plastic Solids," *Int. J. Solids Struct.*, Vol. 36, 1999, pp. 1231–1243.

[27] Sneddon, I. N., "The Relation Between Load and Penetration in the Axisymmetric Boussinesq Problem for a Punch of Arbitrary Profile," *Int. J. Eng. Sci.*, Vol. 3, 1965, pp. 47–57.

[28] Liu, S., Gu, Y., and Huang, H., "A New Area Function for Instrumented Nanoindentation at Extremely Small Contact Depths," *Mater. Sci. Eng. A*, Vol. 528, 2011, pp. 7948–7951.

[29] Pharr, G. M., Oliver, W. C., and Brotzen, F. R., "On the Generality of the Relationship Among Contact Stiffness, Contact Area, and Elastic Modulus During Indentation," *J. Mater. Res.*, Vol. 7, 1992, pp. 613–617.

[30] Johnson, K. L., *Contact Mechanics*, Cambridge University Press, Cambridge, U.K., 1985.

[31] Greenwood, J. A., Johnson, K. L., and Matsubara, E., "A Surface Roughness Parameter in Hertz Contact," *Wear*, Vol. 100, 1984, pp. 47–57.

[32] Fischer-Cripps, A. C., *Nanoindentation*, Mechanical Engineering Series, 2nd ed., Springer, New York, 2004.

[33] Chudoba, T. and Richter, F., "Investigation of Creep Behavior Under Load During Indentation Experiments and Its Influence on Hardness and Modulus Results," *Surf. Coat. Technol.*, Vol. 148, 2001, pp. 191–198.

[34] Barksdale, R. D., *The Aggregate Handbook*, National Stone Association, Washington, D.C., 1996.

[35] *ABQUS User's Manual*; *Version 6.8.* (2008). Hibbt, Karlsson & Sorenson, Inc., Pawtucket, RI.

[36] Goodman, R. E., *Introduction to Rock Mechanics*, 2nd ed., John Wiley and Sons, New York, 1989.